33RD INTERNATIONAL COSMIC RAY CONFERENCE, RIO DE JANEIRO 2013
THE ASTROPARTICLE PHYSICS CONFERENCE

ICRC 2013

An ab initio approach to the modulation of galactic electrons and positrons

N.E. ENGELBRECHT[1], R.A. BURGER[1]

[1] *Center for Space Research, North West University.*

12580996@nwu.ac.za

Abstract: The modulation of galactic electrons and positrons is investigated with an ab initio three-dimensional steady state cosmic-ray modulation code. The effects of turbulence on both the diffusion and drift of these cosmic-rays are treated in a self-consistent manner, utilizing a recent two-component turbulence transport model that yields results in reasonable agreement with observations of turbulence quantities throughout the heliosphere. The sensitivity of computed galactic electron intensities to choices of turbulence parameters pertaining to the dissipation range of the slab turbulence spectrum will be demonstrated, and comparisons of computed electron and positron intensities with spacecraft observations will be made.

Keywords: Turbulence, diffusion, drift, cosmic-ray modulation.

1 Introduction

Low-energy galactic electrons have long been known to be particularly sensitive to the choice of diffusion coefficients employed in the study of their modulation, given their insensitivity to the effects of drifts [25]. Many modulation studies utilise parametrised forms for the diffusion and drift coefficients of these cosmic rays [10, 26]. This study aims to present galactic electron and positron intensities, acquired using the 3D, steady state cosmic-ray modulation code of [6], and incorporating in as self-consistent a way as is currently possible the effects of turbulence.

2 Diffusion and drift coefficients

The scattering theories used in this study to derive electron/positron diffusion coefficients require as inputs expressions for the power spectra of the turbulent fluctuations in the heliospheric magnetic field (HMF). As such, making the assumption of composite turbulence following [3], a total turbulence modal spectrum is specified such that $G(\mathbf{k}) = G^{slab}(k_\parallel)\delta(k_\perp) + G^{2D}(k_\perp)\delta(k_\parallel)$, where $G(\mathbf{k})$ and $G^{2D}(k_\perp)$ respectively denote the slab and 2D modal spectra. The spectral forms used in this study are functions of basic turbulence quantities such as the magnetic variance. To model diffusion coefficients derived using these spectra throughout the heliosphere, these spectra, and hence the turbulence quantities they are functions of, need to be modelled throughout the heliosphere. To this end, the present study employs the two-component turbulence transport model (TTM) of [24]. This model is solved for solar minimum conditions, assuming a Parker HMF, and using boundary conditions chosen so that the results yielded by this model are in fair to good agreement with extant spacecraft observations of turbulence quantities throughout the heliosphere [11].

This study employs the electron/positron parallel mean free path (MFP) expressions presented by [12], which those authors construct from the piecewise analytical expressions derived by [29] from quasilinear theory, assuming the random sweeping model of dynamical turbulence [3]. The slab modal spectrum used by [29] is therefore also used here, and is given by

$$G^{slab}(k_\parallel) = \begin{cases} g_o k_m^{-s},\ |k_\parallel| \le k_m; \\ g_o |k_\parallel|^{-s},\ k_m \le |k_\parallel| \le k_d; \\ g_1 |k_\parallel|^{-p},\ |k_\parallel| \ge k_d. \end{cases} \quad (1)$$

Here k_m is the parallel wavenumber at which the inertial range of the above spectrum commences, k_d the wavenumber associated with the onset of the dissipation range, $g_1 = g_0 k_d^{p-s}$, and

$$g_o = \left[s + \frac{s-p}{p-1} \left(\frac{k_m}{k_d} \right)^{s-1} \right]^{-1} \frac{\delta B_{sl}^2 k_m^{s-1} (s-1)}{8\pi} \quad (2)$$

where s and p respectively denote the spectral indices of the inertial and dissipation ranges on this spectrum. Here it is assumed that s is equal to the Kolmogorov $5/3$ value, and $p = 2.6$, as observed by [27]. Lastly, δB_{sl}^2 denotes the slab variance. The abovementioned electron/positron parallel MFP expression is given by [12]

$$\begin{aligned} \lambda_\parallel &= \frac{3s}{\sqrt{\pi}(s-1)} \frac{R^2}{k_{min}} \left(\frac{B_o}{\delta B_{slab}} \right)^2 \\ &\cdot \left[\frac{1}{4\sqrt{\pi}} + \left(\frac{1}{\Gamma(p/2)} + \frac{1}{\sqrt{\pi}(p-2)} \right) \frac{b^{p-2}}{Q^{p-s} R^s} \right. \\ &+ \left. \frac{2}{\sqrt{\pi}(2-s)(4-s)} \frac{1}{R^s} \right]. \end{aligned} \quad (3)$$

Quantities such as k_m and δB_{sl}^2 are here acquired using the results of the [24] TTM. Two of the dissipation range onset wavenumber k_D models discussed by [18], where k_D is a function of the proton gyrofrequency Ω_{ci} or the ion inertial scale ρ_{ii}, are considered here, as in [12]. [18] test these models by fitting linear regressions to *Wind* data taken at 1 AU. This study, like that of [12], considers the effects of the linear regression models of [18] (i.e. the best fit and fit through origin regressions), extrapolated throughout the heliosphere, on electron/positron modulation. Note also that $R = R_L k_m$, where R_L is the maximal particle gyroradius, $b = v/(\alpha_d V_A)$, v is the particle speed and V_A the Alfén speed. The quantity α_d adjusts dynamical effects, and a value of unity is used here, implying that the underlying turbulence is assumed to be strongly dynamical [3].

The 2D modal spectrum used into derive a perpendicular MFP expression is defined following [22] with an inertial range, a flat energy-containing range, and an 'outer range' displaying a steep decrease at the smallest wavenumbers, as

$$G^{2D}(k_\perp) = g_2 \begin{cases} (\lambda_{out} k_\perp)^q, |k_\perp| < \lambda_{out}^{-1}; \\ 1, \lambda_{out}^{-1} \leq |k_\perp| < \lambda_{2D}^{-1}; \\ (\lambda_{2D} k_\perp)^{-\nu}, |k_\perp| \geq \lambda_{2D}^{-1}. \end{cases} \quad (4)$$

where $g_2 = (C_o \lambda_{2D} \delta B_{2D}^2)/(2\pi k_\perp)$, and

$$C_0 = \left[\left(1 - \frac{q}{1+q} \left(\frac{\lambda_{2D}}{\lambda_{out}} \right) + \frac{1}{\nu - 1} \right) \right]^{-1} \quad (5)$$

with δB_{2D}^2 denoting the 2D variance, $\nu = 5/3$ the spectral index in the inertial range and q the spectral index in the 'inner range', which, based on physical considerations argued by [22], is set to 3. The lengthscale λ_{2D} denotes the 2D bendover scale at which the inertial range commences, while λ_{out} denotes the 2D outerscale, where the energy range commences, such that $\lambda_{out} > \lambda_{2D}$. No observations currently exist for the 2D outerscale, and it is assumed that $\lambda_{out} = 12.5\lambda_{c,2D}$, with $\lambda_{c,2D}$ the 2D correlation scale. The motivation behind this simple dependence is that this choice of 2D outerscale led to reasonably good agreement of modelled galactic proton and antiproton cosmic-ray intensities with spacecraft observations when employed by [11]. Using the above spectrum as an input for the Extended Nonlinear Guiding Center theory of [28], [11] derives an expression for the perpendicular MFP given by

$$\lambda_\perp = \frac{2a^2}{B_o^2} \frac{C_0 \lambda_{2D} \delta B_{2D}^2}{\lambda_\perp} \left[h_{\perp,1} + h_{\perp,2} + h_{\perp,3} \right], \quad (6)$$

where

$$\begin{aligned} h_{\perp,1} &= \frac{\lambda_\parallel \lambda_\perp}{(1+q)\lambda_{out}} {}_2F_1(1, \frac{1+q}{2}, \frac{3+q}{2}; -x^{-2}), \\ h_{\perp,2} &= \sqrt{3\lambda_\parallel \lambda_\perp} \left[\arctan(x) - \arctan(y) \right], \\ h_{\perp,3} &= \frac{3\lambda_{2D}}{(1+\nu)} {}_2F_1(1, \frac{1+\nu}{2}, \frac{3+\nu}{2}; -y^2), \end{aligned}$$

with

$$x = \frac{\sqrt{3}\lambda_{out}}{\sqrt{\lambda_\parallel \lambda_\perp}} \text{ and } y = \frac{\sqrt{3}\lambda_{2D}}{\sqrt{\lambda_\parallel \lambda_\perp}}, \quad (7)$$

The parameter a^2 is a constant set to $1/3$ in this study, after [21]. The above expressions are evaluated numerically using the results yielded by the TTM to model turbulence quantities.

The drift coefficient used in this study is given by [4]

$$\kappa_A = \frac{v}{3} R_L \frac{\Omega^2 \tau^2}{1 + \Omega^2 \tau^2}, \quad (8)$$

with τ a decorrelation rate, and Ω the particle gyrofrequency. [7] propose a parametrized form for the product $\Omega\tau$, given by

$$\Omega\tau = \frac{11}{3} \frac{\sqrt{R_L/\lambda_{c,s}}}{(D_\perp/\lambda_{c,s})^g}, \quad (9)$$

where $g = 0.3\log(R_L/\lambda_{c,s}) + 1.0$, and $D_\perp = (1/2)(D_{sl} + \sqrt{D_{sl}^2 + 4D_{2D}^2})$ the field line random walk diffusion coefficient [20], with $D_{sl} = (\delta B_{sl}^2/2B_o^2)\lambda_{c,s}$ and $D_{2D} = (\lambda_u \sqrt{\delta B_{2D}^2/2})/B_o$. The quantity $\lambda_{c,s}$ is the slab correlation scale, and λ_u the 2D ultrascale [22]. The ultrascale is calculated from the 2D modal spectrum (Eq. 4), following the approach outlined by [22]. The turbulence-reduced drift coefficient proposed by [7] is employed here, with turbulence quantities appearing in the above expressions being modelled using the [24] TTM.

3 Galactic electron and positron modulation results

Modulation results are acquired using a 3D, steady-state numerical modulation code [6, 12]. The electron local interstellar spectrum (LIS) here used is that of langner2001 while the positron LIS is that of [10], assuming a spherical heliosphere with a radius of 100 AU. The effects of a termination shock or heliosheath are not included. This is done because the Oughton2011 TTM was derived assuming an Alfvén speed considerably smaller than the solar wind speed, which is not the case in the heliosheath. Furthermore, a Parker HMF is assumed, using a latitude-dependent solar wind speed modelled with a hyperbolic tangent function that assumes a value of 400 km/s in the ecliptic and 800 km/s over the poles, the tilt angle of the heliospheric current sheet is taken to be 5°, and the current sheet is treated following the approach of [8].

The top panels of Fig. 1 show the computed galactic cosmic-ray electron intensities as functions of kinetic energy at Earth, and their computed latitude gradients at 2 AU, for the extrapolated [18] models for k_D. There is a clear charge-sign dependence in the solutions, with intensities corresponding to $A < 0$ conditions (hence, $qA > 0$) being consistently larger than those corresponding to $A > 0$ conditions. At the highest energies, the choice of k_D has virtually no effect on computed intensities. This is because at these energies the electron parallel MFPs are essentially independent of quantities pertaining to the dissipation range. The intensities yielded by this approach are in reasonable agreement with the high energy observations shown for both magnetic polarity cycles, and at both radial distances considered. The low-energy intensities reported by [23, 19] pertain to a considerable Jovian component and are included only for the purposes of comparison as an upper bound for computed galactic electron intensities. Conclusions can however still be drawn as to the behaviour of low-energy galactic electrons, as the total contribution of this component to the cosmic-ray electron intensity at Earth has been estimated at $\sim 20\%$ [14].

At intermediate to low energies the effects of the different models for k_D become more readily apparent. Both best-fit models lead to spectra that are essentially identical which show a strong charge-sign dependence down to the lowest energies. The fit through origin proton gyrofrequency model for k_D yields intensities that show a clear increase at intermediate energies, following the trend of the observations but remaining below them, and relax towards the no-drift solution (computed for the same model for k_D, as expected when drift effects become unimportant at low energies [25]. Below ~ 0.1 GeV all computed spectra display an E^2 kinetic energy dependence, a hallmark of having re-

laxed to the relativistic adiabatic limit [9]. Spectra computed using the best-fit models for k_D, however, remain in this limit down to the lowest energies shown. These differences in the solutions corresponding to the various models for k_D can be understood in terms of the behaviour of the parallel MFPs in the the outer heliosphere. The fit through origin proton gyrofrequency model yields the smallest values for k_D in the outer heliosphere, and hence the largest values for the electron parallel MFP at low rigidities. The best-fit models yield very similar values for k_D in this region, and consequently very similar parallel MFPs, considerably smaller than those for the fit through origin proton gyrofrequency model. As the ENLGC perpendicular mean free paths scale roughly as $\lambda_{\parallel}^{2/3}$ this also applies equally to their behaviour at lower rigidities, and explains the similarity of the cosmic-ray intensities computed when the best-fit models for k_D are employed. The charge-sign dependence seen at the lowest energies when the best-fit models for k_D are used is then a direct consequence of the fact that, due to the smaller $\lambda_{\perp}$ and $\lambda_{\parallel}$ for these models, drift effects dominate the transport of the galactic electrons at low energies. The computed galactic electron latitude gradients appear to be independent of k_D at the highest rigidities shown. The signs of latitude gradients for $A > 0$ and $A < 0$ are as expected of negatively charged cosmic-rays [16]. The computed $qA > 0$ latitude gradients shown all agree, within uncertainty, with the [15] data point shown. At lower rigidities, the effects of the various models for k_D can clearly be seen, with the results for the fit through origin proton gyrofrequency model relaxing to the no-drift values at the lowest energies shown. The latitude gradients for the best-fit models for k_D are very similar. The disappearance of the latitude gradients computed for the best-fit k_D models below about 0.1 GV is a consequence of the adiabatic cooling of these cosmic-rays [9].

Computed positron intensity spectra at Earth are shown in the bottom left panel of Fig. 1 as functions of kinetic energy. Note that these results are computed using the fit through origin proton gyrofrequency model for k_D. Solutions corresponding to $A > 0$ conditions remain above those for $A < 0$ at higher energies, in line with what is expected of the effects of drift on positively charged cosmic-rays [16]. At the very lowest energies, the $A > 0$ and $A < 0$ spectra relax to a no-drift solution, becoming essentially equal. Furthermore, at the highest energies illustrated in Fig. 1, computed spectra for both magnetic polarities are in good agreement with the observations shown. Below ~ 1 GeV, however, this agreement becomes less good, with computed spectra for $A > 0$ becoming somewhat larger than spacecraft observations at these energies. The bottom right panel of the same figure shows computed positron ratios for both magnetic polarities as functions of kinetic energy, along with observations of this quantity by various experiments as indicated in the legend. Note that the galactic electron intensity spectra used in the calculation of the positron fraction were acquired assuming the same dissipation range quantities as were employed in the computation of the positron spectra shown in the bottom left panel. At the energies shown, the positron fraction during $A > 0$ remains larger than that during $A < 0$. Both computed positron fractions remain well below PAMELA observations at the highest energies, as possible primary high-energy positron sources (see [1]) are not taken into account in the local interstellar spectrum employed. Computed positron fractions for $A > 0$ are in reasonably good agreement with the solar minimum observations shown, falling mostly within the range defined by their uncertainties, but also appears to have a steeper energy dependence than the qualitative trend of the data, leading to over-large computed values for this quantity at lower energies. During $A < 0$, the computed positron fraction also agrees reasonably well with the AESOP data, but falls below the lower-energy PAMELA data. This being noted, the *ab initio* approach appears to yield results in fair agreement with observations of positrons, and the positron fraction, for diffusion and drift coefficients exactly the same as those used to compute galactic electron intensities.

4 Conclusions

In conclusion, an *ab initio* treatment of diffusion and drift can yield computed cosmic-ray intensities in reasonably good agreement with multiple sets of spacecraft observations, and for different cosmic-ray species. The sensitivity of computed intensities to choices made as to turbulence quantities raises the intriguing possibility that cosmic-ray observations at Earth could possibly be used as a diagnostic from which conclusions may be drawn as to the global behaviour of some turbulence quantities.

The financial assistance of the National Research Foundation (NRF) towards this research is hereby acknowledged. Opinions expressed and conclusions arrived at, are those of the author and are not necessarily to be attributed to the NRF.

References

[1] Adriani, O. et al., 2009, Nature, 458, 607-609
[2] Alcaraz, J. et al., 2000, Physics Letters B, 484, 10-22
[3] Bieber, J. W. et al., 1994, The Astrophysical Journal, 420, 294-306
[4] Bieber, J. W., & Matthaeus, W. H. 1997, The Astrophysical Journal, 485, 655-659
[5] Boezio, M. et al., 2000, The Astrophysical Journal, 532, 653-669
[6] Burger, R. A. et al., 2008, The Astrophysical Journal, 674, 511-519
[7] Burger, R. A., & Visser, D. J. 2010, The Astrophysical Journal, 725, 1366-1372
[8] Burger, R. A. 2012, The Astrophysical Journal, 760, 60
[9] Caballero-Lopez, R. A. et al., 2010, The Astrophysical Journal, 725, 121-127
[10] Della Torre, S. et al., 2012, Adv. Space Res., 49, 1587-1592
[11] Engelbrecht, N.E. 2013, On the development and applications of a three-dimensional *ab initio* cosmic-ray modulation model, PhD Thesis, North-West University
[12] Engelbrecht, N. E., & Burger, R. A. 2010, Adv. Space Res., 45, 1015-1025 & Balogh, A. 2005, Adv. Space Res., 35, 625-635
[13] Evenson, P. et al., 1983, The Astrophysical Journal Letters, 275, L15-L18
[14] Ferreira, S. E. S. 2002, The Heliospheric Transport of Galactic Cosmic Rays and Jovian Electrons, PhD Thesis, Potchefstroomse Universiteit vir Christelike Hoër Onderwys
[15] Heber, B. et al., 2008, The Astrophysical Journal, 689, 1443-1447

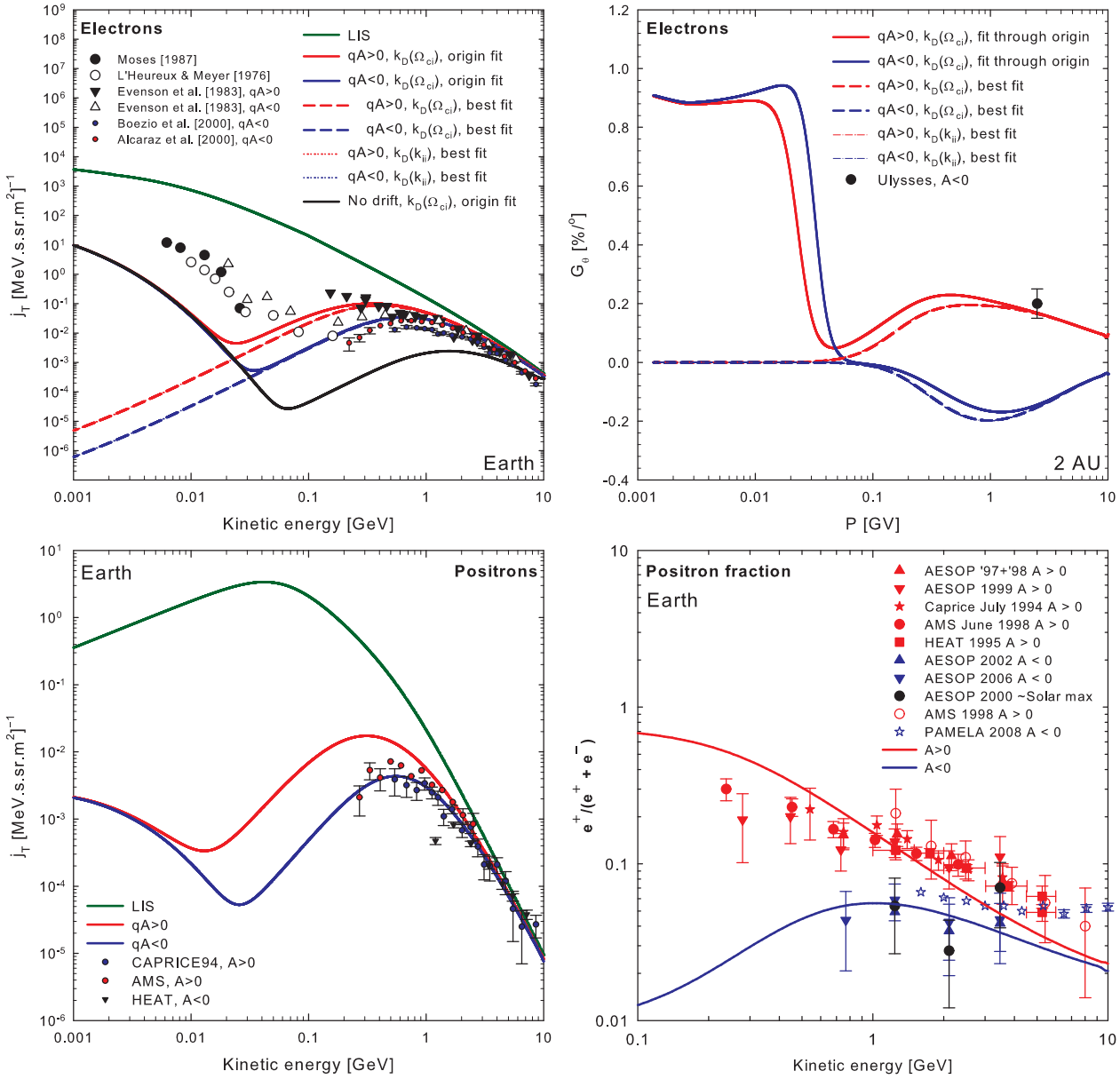

Fig. 1: Computed galactic electron intensities at Earth (top left panel), and latitude gradients at 2 AU (top right panel). Bottom panels show computed galactic positron intensities and the computed positron fraction at Earth. Observational data taken from the references in the legend of the figure.

[16] Jokipii, J. R., & Thomas, B. 1981, The Astrophysical Journal, 243, 1115-1122
[17] Langner, U. W., de Jager, O. C., & Potgieter, M. S. 2001, Adv. Space Res., 27, 517-522
[18] Leamon, R. J. et al., 2000, The Astrophysical Journal, 537, 1054-1062
[19] L'Heureux, J., & Meyer, P. 1976, The Astrophysical Journal, 209, 955-960
[20] Matthaeus, W. H. et al., 1995, Physical Review Letters, 75, 2136-2139
[21] Matthaeus, W. H. et al., 2003, The Astrophysical Journal Letters, 590, L53-L56
[22] Matthaeus, W. H. et al., 2007, The Astrophysical Journal, 667, 956-962
[23] Moses, D. 1987, The Astrophysical Journal, 313, 471-486
[24] Oughton, S. et al., 2011, Journal of Geophysical Research, 116, 8105
[25] Potgieter, M. S. 1996, Journal of Geophysical Research, 101, 24411-24422
[26] Potgieter, M. S., & Ndanganeni, R. R. 2013, Astrophysics and Space Science, 345, 33-40
[27] Smith, C. W. et al., 2006, The Astrophysical Journal Letters, 645, L85-L88
[28] Shalchi, A. 2006, Astronomy and Astrophysics, 453, L43-L46
[29] Teufel, A., & Schlickeiser, R. 2003, Astronomy and Astrophysics, 397, 15-25